


Enhanced anisotropy and study of magnetization reversal in Co/C₆₀ bilayer thin film

Cite as: Appl. Phys. Lett. **115**, 242405 (2019); <https://doi.org/10.1063/1.5096879>

Submitted: 20 March 2019 . Accepted: 23 November 2019 . Published Online: 12 December 2019

Srijani Mallik, Purbasha Sharangi, Biswajit Sahoo, Stefan Mattauch, Thomas Brückel, and Subhankar Bedanta 



View Online



Export Citation



CrossMark

ARTICLES YOU MAY BE INTERESTED IN

[Long-range ferromagnetic ordering in vanadium-doped WSe₂ semiconductor](#)

Applied Physics Letters **115**, 242406 (2019); <https://doi.org/10.1063/1.5131566>

[Observation of large anomalous Nernst effect in 2D layered materials Fe₃GeTe₂](#)

Applied Physics Letters **115**, 212402 (2019); <https://doi.org/10.1063/1.5129370>

[Stack structure and temperature dependence of spin-orbit torques in heterostructures with antiferromagnetic PtMn](#)

Applied Physics Letters **115**, 242404 (2019); <https://doi.org/10.1063/1.5129829>

Lock-in Amplifiers up to 600 MHz



Zurich
Instruments



Enhanced anisotropy and study of magnetization reversal in Co/C₆₀ bilayer thin film

Cite as: Appl. Phys. Lett. **115**, 242405 (2019); doi: [10.1063/1.5096879](https://doi.org/10.1063/1.5096879)

Submitted: 20 March 2019 · Accepted: 23 November 2019 ·

Published Online: 12 December 2019



View Online



Export Citation



CrossMark

Srijani Mallik,¹ Purbasha Sharangi,¹ Biswajit Sahoo,¹ Stefan Mattauch,² Thomas Brückel,^{2,3} and Subhankar Bedanta^{1,a)} 

AFFILIATIONS

¹Laboratory for Nanomagnetism and Magnetic Materials (LNMM), School of Physical Sciences, National Institute of Science Education and Research (NISER), HBNI, P.O.- Jatni 752050, India

²Jülich Centre for Neutron Science (JCNS), Heinz Maier-Leibnitz Zentrum (MLZ), Forschungszentrum Jülich GmbH, Lichtenbergstr. 1, 85748 Garching, Germany

³PGI-4: Scattering Methods Forschungszentrum Jülich GmbH 52425 Jülich, Germany

^{a)}Electronic mail: sbedanta@niser.ac.in

ABSTRACT

The interface between the organic semiconductor (OSC)/ferromagnetic (FM) material can exhibit ferromagnetism due to their orbital hybridization. Charge/spin transfer may occur from the FM to OSC layer leading to the formation of “spinterface,” i.e., the interface exhibiting a finite magnetic moment. In this work, the magnetic properties of the Co/C₆₀ bilayer thin film have been studied to probe the interface between the Co and C₆₀ layer. Polarized neutron reflectivity (PNR) measurement indicates that the thickness and moment of the spinterface are $\sim 2 \pm 0.18$ nm and $0.8 \pm 0.2 \mu_B/\text{cage}$, respectively. The comparison of the magnetization reversal between the Co/C₆₀ bilayer and the parent single layer Co thin film reveals that spinterface modifies the domain microstructure. Further, the anisotropy of the bilayer system shows a significant enhancement (\sim two times) in comparison to its single layer counterpart which is probably due to an additional interfacial anisotropy arising from the orbital hybridization at the Co/C₆₀ interface.

Published under license by AIP Publishing. <https://doi.org/10.1063/1.5096879>

The study of spin-dependent interfacial properties of ferromagnetic (FM)/organic semiconductor (OSC) interfaces has received immense research interest in the last decade.^{1–3} This is due to both their potential applications in organic spintronic devices and the fundamental properties observed upon forming the “spinterface.” Spinterface is the gateway between two layers through which polarized spins can be transferred. It is a special type of interface having properties which are significantly different from their constituent layers.^{4–6} The coupling between a FM and OSC molecule at the interface may promote FM state in the OSC layer.^{7–11} Buckminsterfullerene (C₆₀) is a potential candidate for such spin polarized charge transfer as it is composed of only carbon atoms. This is because it exhibits properties like low spin–orbit coupling (due to lower at. wt.) and correspondingly longer spin lifetime, stability under thermal and mechanical duress, a reasonable mobility of $11 \text{ cm}^2/\text{V s}$, etc.^{7–11} The C atoms present in C₆₀ may undergo the *s-p* hybridization mechanism to lower the total energy of the system. Thus, it is prone to hybridize orbitals with FM materials having unfilled *d* orbitals. For example, Moorsom *et al.* have studied Co/C₆₀ multilayers by polarized neutron reflectometry and

found that magnetic moment can be induced in C₆₀ due to charge transfer.⁷ However, the exact thickness of the spinterface has not been deduced in their study because of interdiffusion between Co and C₆₀. Similarly, C₆₀ monolayers on Fe (001) reveal magnetic polarization of C₆₀ due to the hybridization of C₆₀ and Fe orbitals.⁸ The hybrid interface between Fe and C₆₀ leads to magnetic moments $\mu_S = 0.21$ and $0.27 \mu_B$ per C molecule for C₆₀ layers on Fe(001) and Fe/W(001), respectively.⁹ Recently, the spinterface of about 2 nm thickness in Fe/C₆₀ bilayer system has been observed which exhibits a moment ~ 1.5 to $3 \mu_B$ per cage of C₆₀.¹⁰ The reason behind the charge transfer between the FM and the OSC layer is the *d*_{FM}-*p*_{OSC} orbital hybridization at the interface. It has been also reported that such spinterfaces have a significant effect on the magnetization reversal mechanism and domains of epitaxial Fe/C₆₀ bilayer systems.¹⁰ The aforementioned effects have not been explored so far for Co/C₆₀ systems.

It should be noted that the hybridization between the FM and OSC molecules directly involves the orbitals; therefore, it is expected that the anisotropy of such systems may get modified. It has been reported that the presence of a C₆₀ layer on the Co ultrathin film can

control the anisotropy symmetry of the system through an inverse spin reorientation transition from in-plane to out-of-plane via the local hybridization between C_{60} p_z and Co d_{z^2} orbitals.^{12,13} However, the effect of hybridization on the global anisotropy symmetry for in-plane magnetized thin films has not been explored so far.

In this paper, the magnetization reversal has been studied in terms of domain images for a system having Co/ C_{60} spinterface and compared to that of its parent single layer Co thin film. The induced moment in the interfacial C_{60} layer is quantified by polarized neutron reflectivity measurement. Further, the effect of such magnetically coupled interface on the net anisotropy of the system has been studied using the ferromagnetic resonance technique.

Co and C_{60} layers have been prepared using dc magnetron sputtering and thermal evaporation techniques, respectively, in a multideposition high vacuum chamber manufactured by Mantis Deposition Ltd., UK. The base pressure of the system was better than 5×10^{-8} mbar. The deposition pressure for Co and C_{60} layers was 5×10^{-3} and 1×10^{-7} mbar, respectively. Co and C_{60} layers have been deposited *in situ*, i.e., without breaking the vacuum in between the deposition of two consecutive layers to avoid the oxidation and surface contamination of the Co layer. The rate of depositions of Co and C_{60} layers was 0.02 and ~ 0.01 – 0.013 nm/s, respectively. Before depositing the Co layer, 5 nm of Ta has been deposited as a seed layer using dc sputtering on the Si (100) substrate to promote a better growth of Co. The lattice constant of Ta (a_{Ta}) is more than that of Co (a_{Co}) and less than Si (a_{Si}). As a consequence, the growth of Co is better on Ta than depositing directly on the Si (100) substrate. To prevent oxidation of Co and surface corrosion of C_{60} , a Ta capping layer of 3 nm has been deposited *in situ* for both the samples. The sample structures are as follows:

Sample 1: Si (100)/Ta(5 nm)/Co(10 nm)/Ta(3 nm)

Sample 2: Si (100)/Ta(5 nm)/Co(10 nm)/ C_{60} (12 nm)/Ta(3 nm)

C_{60} has been deposited normal to the substrate. However, the Co target is at 30° angle with respect to the substrate normal due to the in-built geometry of our deposition system. Therefore, a uniaxial anisotropy is expected in our samples due to the oblique angle of deposition.^{10,14–17} The hysteresis loops and the corresponding domain images have been measured at room temperature using magneto-optic Kerr effect (MOKE) based microscopy manufactured by Evico magnetics GmbH, Germany.¹⁸ The hysteresis measurements have been performed within a field range of 20 mT by varying the angle ϕ in longitudinal mode. Here, ϕ denotes the angle between the easy axis and applied field direction. Polarized neutron reflectivity (PNR) has been performed at room temperature on the bilayer film (sample 2) along the easy axis at MARIA reflectometer at FRM II, Garching, Germany.¹⁹ The wavelength (λ) of the neutrons during the PNR measurements has been chosen to be 0.65 nm. The momentum transfer (Q_z) has been measured by rotating the sample in a specific angle range and keeping the wavelength of the neutron (λ) constant. The nonspin flip (NSF) scattering cross sections (R^{++}) and (R^{--}) have been measured where the first and second signs in the scattering cross section correspond to the polarization of the incident and the reflected neutrons, respectively. A small guiding field has been applied to maintain the polarization of the incident neutrons at MARIA. To evaluate the magnetic moment in the single layer sample 1 and to compare the change in magnetization due to the presence of the spinterface, the hysteresis loop has been measured at room temperature within 250 mT

external field using the superconducting quantum interference device (SQUID) magnetometer manufactured by Quantum Design, USA.²⁰ To quantify the anisotropy constants and to observe the effect of the Co/ C_{60} interface on the anisotropy symmetry, ferromagnetic resonance (FMR) measurements have been performed using the Phase FMR spectrometer manufactured by NanOsc AB, Sweden.²¹ The angle dependent FMR measurements have been performed at a fixed frequency of 10 GHz on both the samples by varying ϕ at an interval of 10° .

The angle dependent hysteresis loops for both the samples measured in longitudinal mode at room temperature are shown in Fig. S1. A qualitative figure to understand the anisotropy symmetry of the samples has been plotted by extracting the angle dependent coercivity (H_C) values. The anisotropy symmetry of both the samples is shown in Fig. 1. It should be noted that Co was deposited under oblique angle of incidence in our sputtering chamber. Because of this, the grains of Co are expected to form chain-like structure and become elongated toward a specific direction; therefore, uniaxial anisotropy is observed in the samples.^{10,14–17} The long range dipolar interaction is the main cause of such elongation of grains; as a result, a uniaxial anisotropy is induced in the system.^{22–24} It should be noted that the easy axis of the induced uniaxial anisotropy lies in-plane at 90° angle with respect to the projection of the plume direction. For sample 1, the symmetry of the uniaxial anisotropy is not very profound. A probable cause of the asymmetric shape of the anisotropy symmetry seen in Fig. 1 can be local dispersion in the anisotropy due to the polycrystalline growth of Co on Ta. Due to the polycrystalline nature of the Co layer, misalignment of local anisotropy in between the neighboring grains may be present. Hence, a local decrease in net anisotropy can be observed in those regions.

It should be noted that H_C increases for sample 2 in comparison to sample 1. This can be explained due to the orbital hybridization at the interface of Co/ C_{60} in sample 2. It is expected from the electronic structures of Co and C_{60} that hybridization is probable between d and p orbitals of Co and C atoms, respectively. Due to such hybridization, the C_{60} molecules at the interface may exhibit ferromagnetism which may promote the enhancement in H_C in sample 2. Detailed information on the induced magnetism in C_{60} is discussed later in this paper. The presence of local minima and maxima other than 90° , 270° and 0° , 180° , respectively, in the anisotropy plot (Fig. 1) indicates the

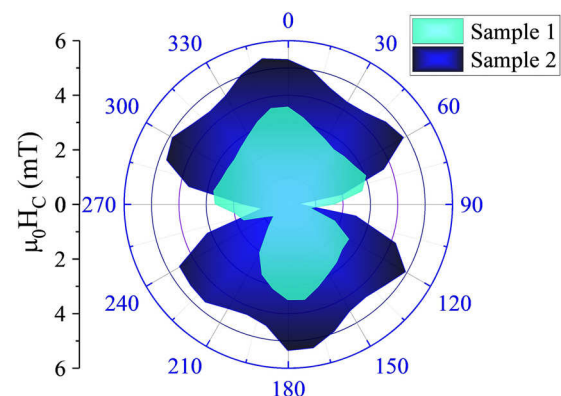


FIG. 1. Angle dependent coercivity (H_C) plots for samples 1 and 2 to compare the anisotropy symmetry.

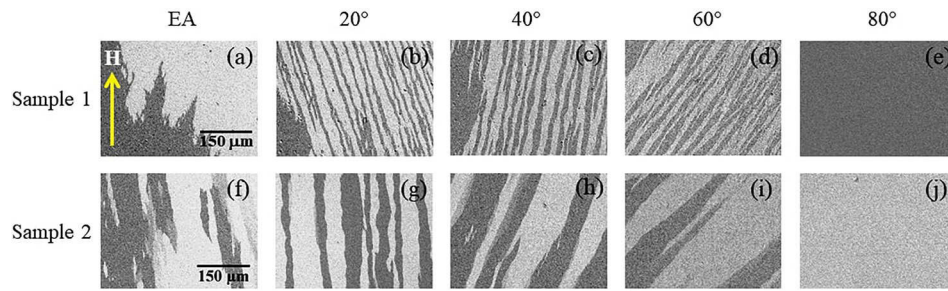


FIG. 2. Domain images near the coercivity for samples 1 and 2 are shown in (a)–(e) and (f)–(j), respectively. The domain images are measured using magneto-optic Kerr effect (MOKE) based microscopy at room temperature in longitudinal mode by varying the angle (ϕ) between the easy axis and the applied field direction. The scale bars of the images for samples 1 and 2 are shown in image (a) and (f), respectively. The applied field direction shown in image (a) was kept constant during all the measurements, and the sample was rotated accordingly.

increase in dispersion or appearance of another anisotropy in sample 2 in comparison to that of the sample 1. The roughness at the Co/C₆₀ interface is expected to be high due to the amorphous growth of C₆₀. As a result, the anisotropy becomes more dispersed in sample 2. Further, the variance in H_C values while changing ϕ is quite prominent for sample 2 (Fig. 1). This indicates that the anisotropy increases in sample 2 in comparison to sample 1 due to the presence of the Co/C₆₀ interface. It should be noted that the hybridization at the Co/C₆₀ interface may promote an interfacial anisotropy which in turn can increase the strength of the uniaxial anisotropy or induce another anisotropy in the bilayer system.

In order to understand the effect of C₆₀ on the magnetization reversal of the bilayer sample, we have performed domain imaging via Kerr microscopy. The domain images captured near the H_C measured along different angles (ϕ) for both the samples are shown in Fig. 2. The first row corresponds to the domain images taken for sample 1. Along the EA, large branch domains are observed. By rotating ϕ away from the EA, the domain size decreases and stripe domains are observed. It is known that branch domains are observed in the samples having poor growth. Similarly, stripe domains are the characteristics of films having dispersed uniaxial anisotropy due to strain.^{25–27} Therefore, due to the polycrystalline growth of Co, branch and stripe domains are observed for different angles. In the case of thin films having well defined uniaxial anisotropy, the domain size decreases monotonically from EA toward HA. However, due to the presence of dispersion in anisotropy symmetry, the domain size increases in between $30^\circ < \phi < 60^\circ$. The variation of average domain widths with respect to ϕ is shown in Fig. S2 of the [supplementary material](#). It should be noted that the domain widths are calculated by taking the average of the width of the branches/stripes measured at several positions of an image. Therefore, the source of error is the systematic error in the measurement, i.e., the least count of the measuring tool. As discussed earlier, the dispersion in anisotropy can be attributed to the fact that the growth of Co is polycrystalline on Ta in our samples.

The second row of Fig. 2 corresponds to the domain states measured for sample 2 for different angles of rotation (ϕ). For this sample also, the nature of the domains stipulates dispersion in the anisotropy due to the presence of Co/C₆₀ interface. However, the increase in domain size in the bilayer sample indicates the presence of orbital hybridization at the Co/C₆₀ interface. For $\phi > 70^\circ$, domains are not observed during the reversal as it happens probably via coherent

rotation. Therefore, a gradual change in the contrast has been observed for $\phi > 70^\circ$ while the field is swept from the positive to negative saturation. Similar to the single layer sample 1, the domain width increases away from EA for the bilayer sample 2. Due to the presence of more dispersion or another anisotropy contribution in sample 2, the domain width at $\phi = 40^\circ$ becomes similar to that of at EA. The change in the domain width with respect to ϕ for sample 2 is depicted in Fig. S2 of the [supplementary material](#). In order to endorse the reproducibility of the results, three sets of samples with similar growth conditions have been measured and verified.

PNR has been performed on sample 2 to quantify the induced moment in C₆₀ and thickness of the spinterface. Figure 3(a) shows the PNR data and the corresponding fits measured at positive saturation ($\mu_0 H = 100$ mT) of the sample at room temperature for sample 2. The red and blue open circles represent the data obtained for the R^{++} and R^{--} reflectivities, respectively. The data have been fitted using GenX software²⁸ which is based on Parratt formalism.²⁹ The sample structure obtained from the best fit is shown in Fig. 3(b) with thicknesses extracted for all the layers. The figure of merit of the fit is less than 8×10^{-2} . From the fitting, it has been observed that the Co layer exhibits a magnetic moment of $1.6 \pm 0.01 \mu_B/\text{atom}$. The magnetic moment of the single layer Co sample 1 has been calculated to be $1.7 \pm 0.03 \mu_B/\text{atom}$ from the SQUID loop (Fig. S3 of the [supplementary material](#)). Therefore, a reduction of $\sim 6\%$ of magnetic moment in

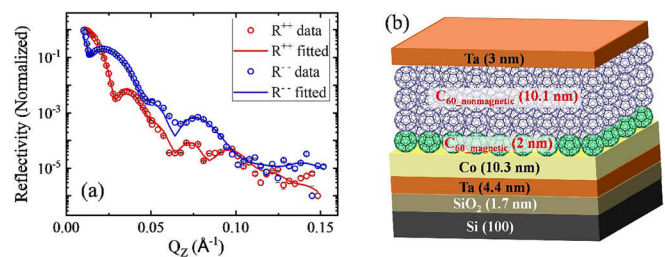


FIG. 3. (a) Polarized neutron reflectivity (PNR) data and the corresponding fits for sample 2. The red and blue open circles represent the data measured for the R^{++} and R^{--} channels, respectively. The solid lines correspond to their respective fits. The measurement was performed at the saturation state at room temperature. (b) A schematic representation of the sample structure obtained by fitting the PNR data are shown in (a). The numbers written in brackets in each layer correspond to the fitted thickness of the respective layer.

Co is observed in the bilayer sample. On top of the Co layer, $\sim 2 \pm 0.18$ nm of pure C_{60} shows a magnetic moment of $0.8 \pm 0.2 \mu_B/\text{cage}$. Further, rest of the 10 ± 0.11 nm of C_{60} exhibits its inherent diamagnetic behavior. The induction of moment in C_{60} cage and loss of moment in Co can be explained due to the hybridization between d_{Co} and $p_{C_{60}}$ orbitals. The unpaired electrons from d orbital of Co atom can be transferred to the p orbital of C atom leading to hybridization. It is highly probable that the density of states of the C_{60} gets strongly modified at the interface resulting in induced ferromagnetism in fullerene.^{4,5} It should be noted that the thickness of the nonmagnetic C_{60} layer does not contribute to the magnetic properties of the system.³⁰ The PNR measurement near the coercive field (Fig. S4 of the [supplementary material](#)) elucidates the antiparallel coupling between C_{60} and Co layer at the interface. In this case, 17% of the Co spins are in reversed state and rest are along the field direction. However, 63% of the magnetic C_{60} spins point in the reverse direction. Therefore, it has been confirmed from the PNR measurement that the change in domain structure, and the anisotropy symmetry discussed earlier is a result of the formation of spinterface between Co and C_{60} .

To quantify and compare the anisotropy in the samples, angle dependent ferromagnetic resonance (FMR) measurement has been performed (Fig. S5 in the [supplementary material](#)). The angle (ϕ) has been rotated in 10° interval for both the samples at a constant frequency of 10 GHz. The corresponding resonance field (H_{res}) has been recorded for each angle. Figure 4 shows the H_{res} vs ϕ data (open black circles for sample 1 and solid red circles for sample 2) and corresponding fits (black solid line for sample 1 and red solid line for sample 2) for both the samples. The energy equation for a system having uniaxial anisotropy can be written as³¹

$$E = -HM_S[\sin \theta \sin \theta_M \cos(\phi_M - \phi) + \cos \theta \cos \theta_M] - 2\pi M_S^2 \sin^2 \theta_M + K_U \sin^2 \theta_M + K_1 \sin^2 \theta_M \sin^2 \phi_M. \quad (1)$$

Here, ϕ is the in-plane angle between the easy axis and the applied field direction. ϕ_M is the in-plane angle between the easy axis and the projection of magnetization. θ and θ_M are the angles between the z-axis with respect to the applied field direction and the magnetization direction, respectively (see the schematic shown in Fig. S6 in the

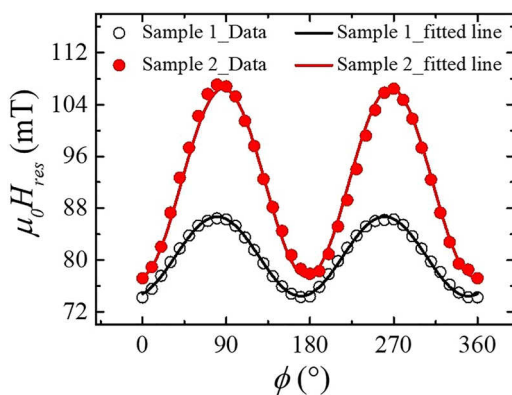


FIG. 4. Angle dependent resonance field (H_{res}) plot for samples 1 (open circles) and 2 (solid circles) to evaluate the anisotropy constants of the system. The FMR measurements were performed at room temperature by keeping the measurement frequency constant at 10 GHz.

[supplementary material](#)). However, θ_M and θ are considered to be 90° as both the magnetization and the field direction lie in the sample plane. Here, the first term of Eq. (1) corresponds to the total Zeeman energy of the system. Due to the interaction of the external magnetic field (H) and the total magnetization of the sample (M_S), the in-plane and out-of-plane components of Zeeman energy are $H \sin \theta M_S \sin \theta_M \cos(\phi_M - \phi)$ and $H \cos \theta M_S \cos \theta_M$, respectively. Further, The demagnetization field is proportional to the magnetic free pole density and can be expressed as $2\pi M_S^2 \sin^2 \theta_M$. The last two terms of Eq. (1) correspond to the uniaxial magnetocrystalline anisotropy energy where K_1 is the in-plane uniaxial anisotropy constant and K_U is the perpendicular contribution of the anisotropy.

The dispersion relation, i.e., the fitting equation to evaluate the strength of the anisotropies present in both the samples, can be derived from Eq. (1) and can be written as³¹

$$(\omega/\gamma)^2 = [H \cos(\phi_M - \phi) - h_U + h_1 \sin^2 \phi_M] [H \cos(\phi_M - \phi) - h_1 + 2h_1 \sin^2 \phi_M], \quad (2)$$

where h_1 is the in-plane anisotropy field and can be expressed as $h_1 = 2(K_1/M_S)$. By fitting the angle dependent H_{res} values (Fig. 4) with Eq. (2), the anisotropy constant K_1 is extracted to be 8.78×10^3 and $1.71 \times 10^4 \text{ J/m}^3$ for samples 1 and 2, respectively. Therefore, it is concluded that the anisotropy increases by two times in the Co/ C_{60} bilayer sample 2 than that of the single layer Co sample 1. Hence, the orbital hybridization at the interface of Co and C_{60} may lead to deformation/elongation of the shape of orbitals which in turn promotes the enhancement of global anisotropy in the bilayer system by probably inducing an extra interfacial anisotropy. The origin and nature of this interfacial anisotropy need to be elucidated by future density functional theory calculations.

In summary, the magnetic properties of bilayer Co/ C_{60} sample have been studied and compared with its parent single layer Co thin film in this paper. Formation of $\sim 2 \pm 0.18$ nm spinterface is observed at the Co/ C_{60} interface which exhibits $0.8 \pm 0.2 \mu_B/\text{cage}$ magnetic moment. The domain size as well as the coercivity of the bilayer sample increases due to the presence of the spinterface. The anisotropy is enhanced by two times in the bilayer sample in comparison to its single layer counterpart due to the $p-d$ orbital hybridization between the C and Co atoms. The possibility of tuning the magnetic anisotropy might have a profound impact on improving the versatility of devices like magnetic tunnel junctions.

See the [supplementary material](#) for the angle dependent Kerr loops (Fig. S1), domain width comparison (Fig. S2), M-H loops from SQUID measurement (Fig. S3), PNR data near the coercive field (Fig. S4), angle dependent FMR spectra (Fig. S5), and schematic for geometry of the angle dependent FMR measurement (Fig. S6).

The authors thank the Department of Atomic Energy and Department of Science and Technology-Science and Engineering Research Board (Nos. SB/S2/CMP-107/2013 and EMR/2016/007725), Government of India for providing the financial support to carry out the experiments. The authors also thank the Department of Science and Technology, India (No. SR/NM/Z-07/2015) for the financial support for performing the neutron experiments and Jawaharlal Nehru Centre for Advanced Scientific Research (JNCASR) for managing the project.

REFERENCES

- ¹V. A. Dediu, L. E. Hueso, I. Bergenti, and C. Taliani, *Nat. Mater.* **8**, 707 (2009).
- ²N. Atodiresi, J. Brede, P. Lazic, V. Caciuc, G. Hoffmann, R. Wiesendanger, and S. Blügel, *Phys. Rev. Lett.* **105**, 066601 (2010).
- ³C. Barraud, P. Seneor, R. Mattana, S. Fusil, K. Bouzehouane, C. Deranlot, P. Graziosi, L. Hueso, I. Bergenti, and V. Dediu, *Nat. Phys.* **6**, 615 (2010).
- ⁴S. Sanvito, *Nat. Phys.* **6**, 562 (2010).
- ⁵F. Djeghloul, F. Ibrahim, M. Cantoni, M. Bowen, L. Joly, S. Boukari, P. Ohresser, F. Bertran, P. Le Fevre, P. Thakur *et al.*, *Sci. Rep.* **3**, 1272 (2013).
- ⁶S. Steil, N. Großmann, M. Laux, A. Ruffing, D. Steil, M. Wiesenmayer, S. Mathias, O. L. A. Monti, M. Cinchetti, and M. Aeschlimann, *Nat. Phys.* **9**, 242 (2013).
- ⁷T. Moorsom, M. Wheeler, T. M. Khan, F. A. Ma'Mari, C. Kinane, S. Langridge, D. Ciudad, A. Bedoya-Pinto, L. Hueso, G. Teobaldi *et al.*, *Phys. Rev. B* **90**, 125311 (2014).
- ⁸T. L. A. Tran, P. K. J. Wong, M. P. de Jong, W. G. van der Wiel, Y. Q. Zhan, and M. Fahlman, *Appl. Phys. Lett.* **98**, 222505 (2011).
- ⁹T. L. A. Tran, D. Çakir, P. K. J. Wong, A. B. Preobrajenski, G. Brocks, W. G. van der Wiel, and M. P. de Jong, *ACS Appl. Mater. Interfaces* **5**, 837 (2013).
- ¹⁰S. Mallik, S. Mattauch, M. K. Dalai, T. Brückel, and S. Bedanta, *Sci. Rep.* **8**, 5515 (2018).
- ¹¹F. Djeghloul, M. Gruber, E. Urbain, D. Xenioti, L. Joly, S. Boukari, J. Arabski, H. Bulou, F. Scheurer, F. Bertran *et al.*, *J. Phys. Chem. Lett.* **7**, 2310 (2016).
- ¹²K. Bairagi, A. Bellec, V. Repain, C. Chacon, Y. Girard, Y. Garreau, J. Lagoute, S. Rousset, R. Breitwieser, Y. C. Hu *et al.*, *Phys. Rev. Lett.* **114**, 247203 (2015).
- ¹³K. Bairagi, A. Bellec, V. Repain, C. Fourmental, C. Chacon, Y. Girard, J. Lagoute, S. Rousset, L. Le Laurent, A. Smogunov, and C. Barreteau, *Phys. Rev. B* **98**, 085432 (2018).
- ¹⁴S. Mallik, N. Chowdhury, and S. Bedanta, *AIP Adv.* **4**, 097118 (2014).
- ¹⁵S. Mallik, S. Mallick, and S. Bedanta, *J. Magn. Magn. Mater.* **428**, 50 (2017).
- ¹⁶S. Mallik and S. Bedanta, *J. Magn. Magn. Mater.* **446**, 270 (2018).
- ¹⁷S. Mallick, S. Mallik, B. B. Singh, N. Chowdhury, R. Gieniusz, A. Maziewski, and S. Bedanta, *J. Phys. D: Appl. Phys.* **51**(27), 275003 (2018).
- ¹⁸See <http://evico-magnetics.de/> for the technical details of the Kerr microscope used in this paper for domain imaging.
- ¹⁹S. Mattauch, A. Koutsoubas, U. Rücker, D. Korolkov, V. Fracassi, J. Daemen, R. Schmitz, K. Bussmann, F. Suxdorf, M. Wagener *et al.*, *J. Appl. Cryst.* **51**, 646 (2018).
- ²⁰See <https://www.qdusa.com/products/mpms3.html> for the technical details of the SQUID used in this paper.
- ²¹See <http://www.nanosc.se/phasefmr.html> for the technical details of the FMR instrument used in this paper.
- ²²S. Cherifi, R. Hertel, A. Locatelli, Y. Watanabe, G. Potdevin, A. Ballestrazzi, M. Balboni, and S. Heun, *Appl. Phys. Lett.* **91**, 092502 (2007).
- ²³J. L. Bubendorff, S. Zabrocki, G. Garreau, S. Hajjar, R. Jaafar, D. Berling, A. Mehdaoui, C. Pirri, and G. Gewinner, *Europhys. Lett.* **75**, 119 (2006).
- ²⁴Y. Shim and J. G. Amar, *Phys. Rev. Lett.* **98**, 046103 (2007).
- ²⁵A. Hubert and R. Schäfer, *Magnetic Domains* (Springer 1998).
- ²⁶H. Kronmüller, M. Fähnle, M. Domann, H. Grimm, R. Grimm, and B. Gröger, *J. Magn. Magn. Mater.* **13**, 53 (1979).
- ²⁷A. Hubert, *J. Magn. Magn. Mater.* **6**, 38 (1977).
- ²⁸See <http://genx.sourceforge.net> for detailed information related to the software.
- ²⁹L. G. Parratt, *Phys. Rev.* **95**(2), 359 (1954).
- ³⁰S. Mallik, A. S. Mohd, A. Koutsoubas, S. Mattauch, B. Satpati, T. Brückel, and S. Bedanta, *Nanotechnology* **30**, 435705 (2019).
- ³¹R. Gieniusz, L. T. Baczewski, Z. Kurant, A. Maziewski, and A. Wawro, *J. Magn. Magn. Mater.* **310**, 2198 (2007).